Astron. Astrophys. 325, 623–630 (1997)

ASTRONOMY AND ASTROPHYSICS

# Phase resolved X-ray spectra of Vela X-1

**P. Kretschmar[1,5], H. C. Pan[2], E. Kendziorra[1], M. Maisack[1], R. Staubert[1], G. K. Skinner[2], W. Pietsch[3], J. Trümper[3], V. Efremov[4], and R. Sunyaev[4]**

[1] Institut für Astronomie und Astrophysik – Astronomie, D-72076 Tübingen, Germany
[2] School of Physics and Space Research, University of Birmingham, Edgbaston, Birmingham B15 2TT, UK
[3] Max-Planck-Institut für Extraterrestrische Physik, D-85470 Garching, Germany
[4] Space Research Institute, Moscow 117296, Russia
[5] Integral Science Data Center, CH-1290 Versoix, Switzerland

Received 14 October 1996 / Accepted 7 April 1997

**Abstract.** Combining simultaneous observations of Vela X-1 by the instruments HEXE and TTM on Mir-Kvant, we have analyzed pulse profiles and pulse phase resolved spectra over a broad energy band (2–120 keV). The pulse profiles show the well known transition from a complex shape at low energies to a double peak structure at energies $\gtrsim$20 keV. The high-energy lightcurves exhibit strong pulse-to-pulse variations. We find indications for spectral features at $\sim$23 and $\sim$45 keV in the phase averaged spectra, which can be interpreted as the fundamental and first harmonic cyclotron resonances, but we caution that the first feature coincides with the spectral cutoff of the continuum spectra used. Pulse phase resolved spectroscopy shows that the shape of the continuum spectrum varies significantly with pulse phase and that the cyclotron features are mainly visible in one of the two pulses seen at high energies.

**Key words:** pulsars: individual: Vela X-1 – stars: magnetic fields – X-rays: stars

## 1. Introduction

Vela X-1 is an eclipsing high-mass X-ray binary consisting of an early type supergiant and a pulsar, having an orbital radius of about 1.7 $R_*$ ($\sim$53 $R_\odot$) with a period of 8.964 days (Nagase et al. 1986). The X-ray pulsar is accreting from the intense stellar wind emanating from the companion, which is close to filling its Roche lobe.

The pulse period of $\sim$283 s has been found to vary on all timescales from days to years since the first observations in 1975. These variations can be described by a random walk in pulse frequency (Deeter et al. 1989), a typical behaviour for a wind-accreting source. The average pulse profile changes from a complex pattern with up to five peaks at energies $\lesssim$10 keV to a double peak structure at energies beyond $\sim$20 keV (see e.g. Raubenheimer 1990). Staubert et al. (1980) found significant pulse-to-pulse variations at energies 18–50 keV. Profiles averaged over many periods are, however, quite stable.

The continuum photon spectrum of Vela X-1 can be described by a power law with an exponential cutoff beyond $\sim$20 keV. As the neutron star is deeply embedded in the dense stellar wind, the X-ray spectrum shows considerable photoelectric absorption at lower energies, varying with orbital phase but also sometimes erratically on short timescales (e.g. Haberl & White 1990). Reprocessing of the pulsar's radiation gives rise to a strong iron fluorescence emission line at $\sim$6.4 keV and an absorption edge at $\sim$7.2 keV (Nagase et al. 1986). Below $\sim$3 keV sometimes a soft excess is observed (Lewis et al. 1992, Pan et al. 1994). Early evidence for cyclotron line features at $\sim$27 and $\sim$54 keV in the phase-averaged spectra has been presented by Kendziorra et al. (1992) and Makishima et al. (1992) and now more recently by Kretschmar et al. (1996).

*Send offprint requests to*: Peter.Kretschmar@obs.unige.ch

## 2. Observations

HEXE and TTM are part of the broadband X-ray observatory KVANT, docked to the Mir space station. The two detectors are coaligned and are operated simultaneously.

TTM is a coded mask camera with a proportional counter sensitive in the energy range 2–25 keV and a sensitive area of $\sim$300 cm$^2$. The field of view is $7.5^\circ \times 7.5^\circ$ FWHM, with an angular resolution of 3 arcmin. The energy resolution is 18% at 6 keV (Brinkman et al. 1985).

HEXE consists of four individual phoswich detectors sensitive in the energy range 20–200 keV, providing a total effective area of 750 cm$^2$. The field of view is defined by two honeycomb tungsten collimators with a triangular response function of $1.6^\circ \times 1.6^\circ$ FWHM. They can be tilted independently by $2.3^\circ$ to allow simultaneous source and background measurements. The energy resolution is $\approx$30% (FWHM) at 60 keV (Reppin et al. 1985).

**Table 1.** Overview of the TTM/HEXE observations.

| Date | JD of centre of observation | Orbital phase [2)] | Integration time [1)] | Pulse Period [2)] | Total count rate 11–40 keV [3)] |
|---|---|---|---|---|---|
| 20.11.88 | 2447486.32 | 0.77–0.79 | 3116 s | 283.28±0.05 s | 672±6 cts/s |
| 25.11.88 | 2447491.29 | 0.31–0.33 | 2078 s | 283.23±0.07 s | 566±7 cts/s |
| 26.11.88 | 2447492.34 | 0.45–0.46 | 2691 s | 283.12±0.12 s | 426±5 cts/s |
| 13.01.91 | 2448270.24 | 0.22–0.23 | 2486 s | 283.33±0.12 s | 841±7 cts/s |

| Ephemeris used: | |
|---|---|
| $T_{\pi/2}$ | = JD 2444279.047 |
| $P_{\rm orb}$ | = 8.96442 d |
| $a_x \sin i$ | = 113.0 lt-sec |
| $\epsilon$ | = 0.089 |
| $\Omega_{\rm peri}$ | = 150.6deg |

[1)] Effective integration time on source

[2)] Using the ephemeris of Nagase (1989). Parameters are given in the table to the right.

[3)] Data are from both instruments and are not affected by photoelectric absorption

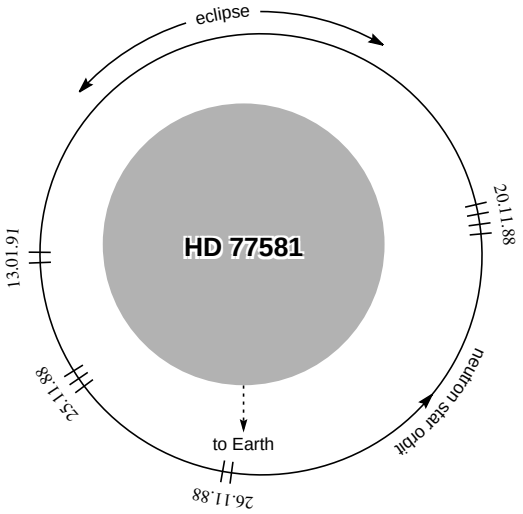


**Fig. 1.** Sketch of the Vela X-1 system. The relative movement of HD 77581 was neglected. Ticks mark the approximate position of the pulsar during the individiual observations using the ephemeris from Nagase (1989) (see Table 1).

Mir-KVANT observations consist of data acquisition intervals of 10–30 minutes duration each. Background observations are either done by rocking the whole spacecraft periodically between source and background (source-free) pointings or – for HEXE – by rocking the collimator halves alternately.

Vela X-1 was observed repeatedly by the Mir-KVANT observatory. We were able to derive joint pulse phase resolved spectra of Vela X-1, covering the energy range 2–120 keV, from four days of observations. The overall source flux varied significantly from one observation to the next (see Table 1).

## 3. Data analysis

### *3.1. HEXE*

Accumulated pulse height spectra of the individual observations were screened for corrupted data and corrected for electronic and telemetry deadtime effects. Background subtraction involved a background model, making use of a proportionality between the detector background and the countrate of the plastic anticoincidence shields or the electronic deadtimes (Döbereiner et al. 1994).

The barycentric photon arrival times were used to establish pulse periods for the individual observations by epoch folding. Using this, background subtracted energy resolved lightcurves and pulse profiles were produced. Pulse phase resolved spectra were derived from these pulse profiles.

### *3.2. TTM*

For TTM the source position in the FOV was first determined from the complete observation. Then separate images were created for each energy channel and time slice and the flux found using the previously determined source position. Background subtraction is done as part of the image reconstruction process.

The pulse periods and phase zero times for time resolved analysis were taken from HEXE data, since its time resolution is better than that of TTM. Because of the problems in image reconstruction from scarce data, pulse profiles with fine phase resolution were only produced in two broad energy bands and light curves of individual pulses were not created at all from the TTM data.

### *3.3. Combined data*

The intercalibration of the instruments was checked individually for each derived pair of instrument spectra by dividing the respective countrates by countrate spectra of the Crab nebula, which was used for calibration of both detectors (Skinner et al. 1991).

For spectral analysis, models were fitted simultaneously to both instrument spectra. The uncertainties of the fit parameters were estimated by calculating $\chi^2$ contour maps and determining the parameter intervals for which $\chi^2 \leq \chi^2_{\rm min} + X$, with $X$ a function of the requested confidence and the number of free parameters in the fit.

A small drift in the energy calibration of TTM required the use of a slightly different response matrix for this instrument in the analysis of the 1991 observations.

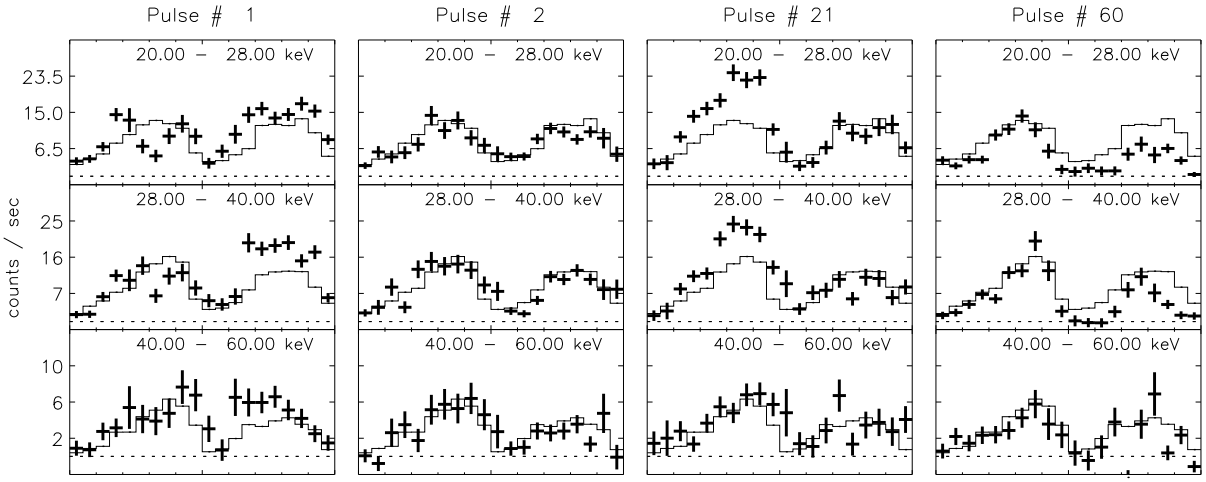


**Fig. 2.** Individual pulse trains from the lightcurves of Nov 20, 1988 in comparison with the average pulse profile (solid histogram) of that day.

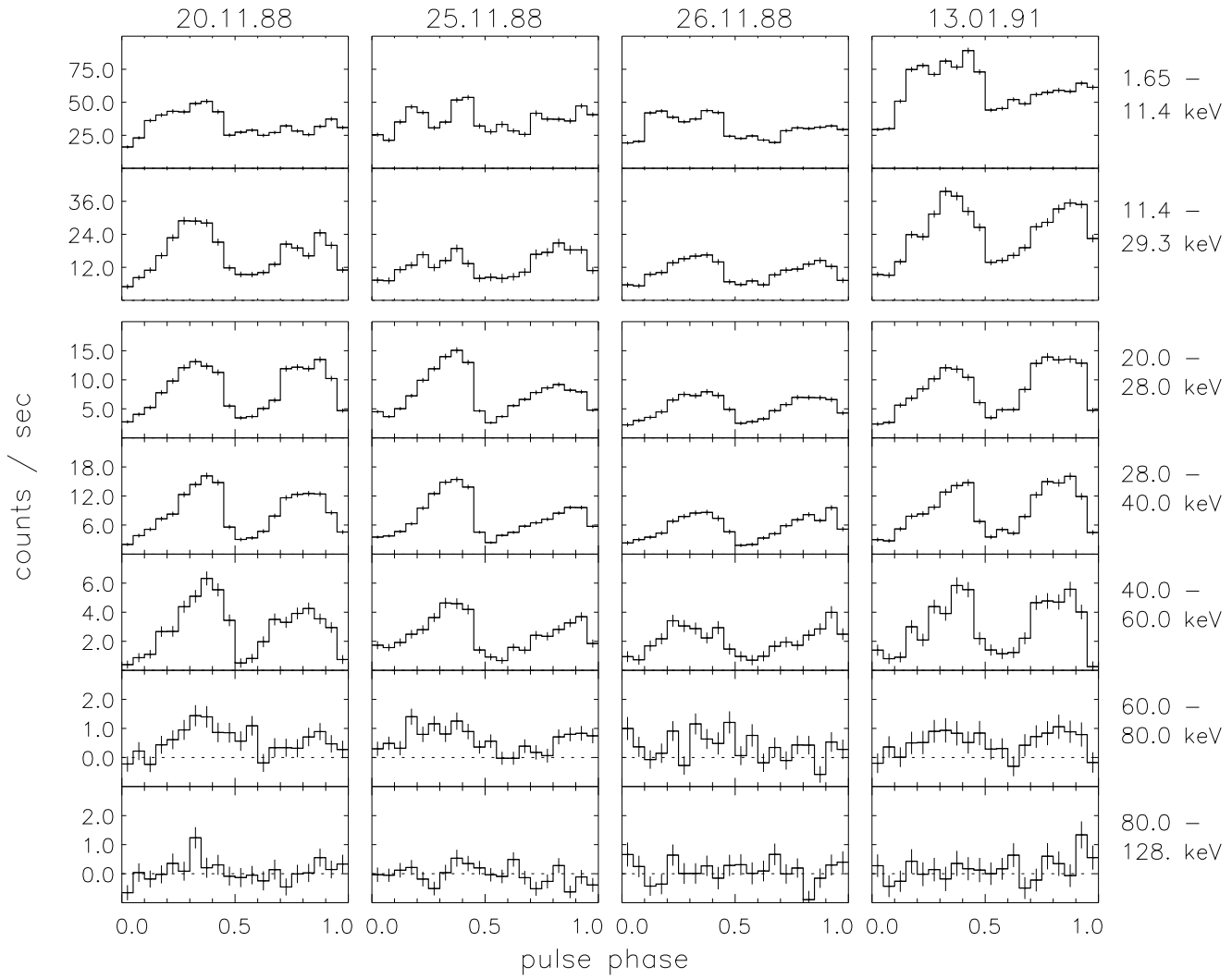


**Fig. 3.** Vela X-1 background subtracted pulse profiles. TTM profiles are displayed in the two upper panels, the corresponding HEXE profiles are plotted below.

## 4. Pulsations

Vela X-1 is known to be far from a steadily emitting source with flux variations on all timescales, including significant variations from one pulse to the other (Staubert et al. 1980, Nagase et al. 1984). Examples of this variability in our own observations are given in Fig. 2. At lower energies these variations have sometimes been explained by variable absorption in clumpy material surrounding the neutron star (Becker et al. 1978). The variations at higher energies indicate that an inhomogenuous accretion flow persists all the way down to the emission regions.

The average pulse profiles of the four days of observation vary also significantly in shape (see Fig. 3). Except for the overall flux variation this change in shape may be due to the relatively short integration times (7–12 pulse periods) and therefore incomplete averaging of the erratic variations.

Assuming a random scatter in the fluxes $\Phi_i$ of the lightcurve bins contributing to a given phase bin, the empirical variance $\sigma^2 = \left(1/n-1\right)\sum_{i=1}^{n}\left(\Phi_i-\bar{\Phi}\right)^2$ can be taken as an estimate of the intrinsic uncertainty of the flux $\Phi_i$ of the $i$th bin due the source variability.

Using this estimate, all four high energy pulse profiles are consistent with the assumption of a common basic shape (scaled by the varying overall source-flux) and erratic variations of individual pulse trains around this mean. All in all the profiles display the expected behaviour with a double peak at higher energies and a more complex structure below $\sim$11 keV.

## 5. Energy spectra

### *5.1. Phase averaged spectra*

As a first step of the spectral analysis, various theoretical model spectra were fitted to the phase averaged spectra of the individual observations. In all cases the photoelectric absorption and the contribution from an iron emission line at 6.4 keV with a fixed width of 0.3 keV were included.

The well known soft-excess for observations with high $N_{\rm H}$ is noticeable in the first observation (Nov 20, 1988) where it somewhat affects the best-fit parameters for $N_{\rm H}$ and the continuum. Since we could not sensibly constrain any model parameters to describe it and the uncertainties in the low energy continuum are quite large anyhow (see Fig. 5 and Table 3), we ignored this effect for our modeling.

The only continuum models which came close to describing the observed countrates were the power law with an exponential cutoff and three comptonized models (Lamb & Sanford 1979, Sunyaev & Titarchuk 1980, Becker & Begelman 1986). The results are summarized in the first part of Table 2. Three spectral models (single power law, thermal bremsstrahlung and pure exponential) can be firmly excluded.

Regardless of the continuum used, some persistent features were present in the fit residuals (see Fig. 4), with the possible exception of the (low flux) observation of Nov 26, 1988. These features varied in position and strength from observation to observation, which complicated a definite identification, but proved that they were not due to problems with the response matrices used. This prompted us to include cyclotron scattering lines (often called absorption lines) into our models.

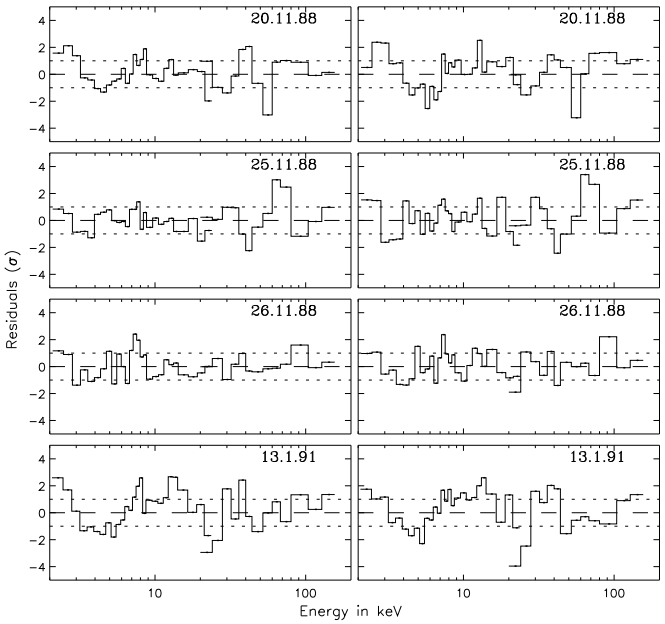


**Fig. 4.** Residuals of fitting a power law with an exponential cutoff to phase averaged spectra (left) and the spectra corresponding to the main pulse (right).

**Table 2.** Results ($\chi^2_{\rm red}$) of fitting different models to the phase averaged source spectra. The models used are explained in the text. The $F$-test probability given in the last row is for the PowExp continuum.

| Model | d.o.f. | 20.11.88 | 25.11.88 | 26.11.88 | 13.01.91 |
|---|---|---|---|---|---|
| continuum spectra without lines: | | | | | |
| Co-LS79 | 35 | 2.58 | 5.32 | 2.27 | 1.93 |
| Co-ST80 | 35 | 2.13 | 4.78 | 2.85 | 3.40 |
| Co-BB86 | 35 | 1.87 | 4.34 | 1.87 | 1.65 |
| PowExp | 34 | 1.50 | 1.25 | 0.98 | 2.53 |
| including cyclotron lines: | | | | | |
| Co-LS79 | 32 | 2.39 | 2.61 | 1.57 | 1.08 |
| Co-ST80 | 32 | 1.37 | 2.21 | 1.63 | 1.03 |
| Co-BB86 | 32 | 1.10 | 1.30 | 1.37 | 0.94 |
| PowExp | 31 | 0.96 | 0.85 | 0.85 | 1.09 |
| $F$-Test Prob. [%] | | 0.07 | 0.18 | 70.1 | 9E−4 |

We used two coupled lines in the form proposed by Tanaka (1986), with the fundamental in the range 15–35 keV. The analytic form is given in Appendix A. Due to the coarse energy resolution of the instruments, line width and depth could not sensibly be determined independently of each other. A fixed width of 1.5 keV (HWHM) was adopted, which is consistent with all individual observations.

Including cyclotron line features improves the fit significantly for three of the four data sets – the exception is the observation of Nov 26, 1988 which is already described well by a power law with an exponential cutoff. For the others, the $F$-test (Bevington & Robinson 1992) gives a probability $<0.2\%$

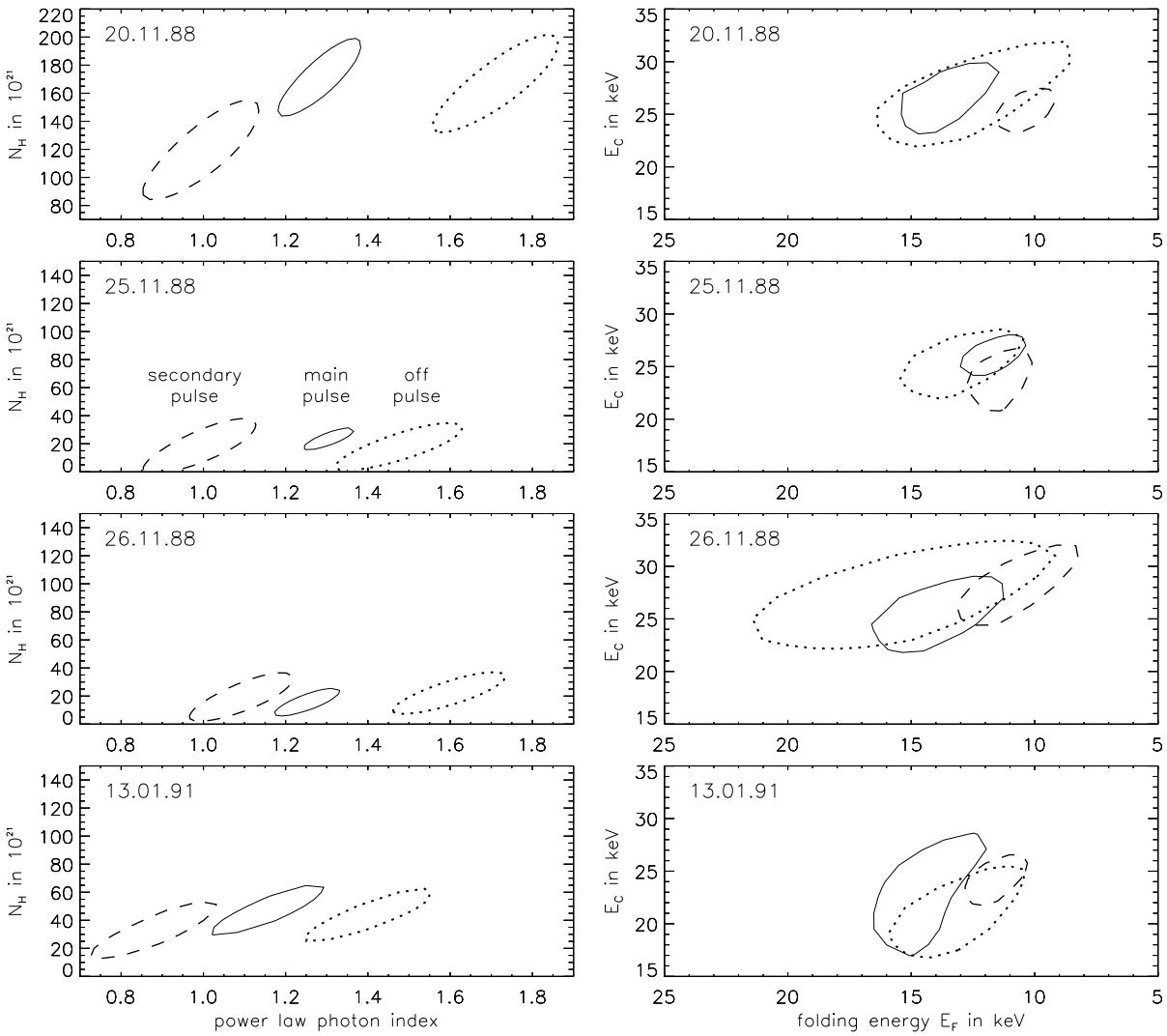


**Fig. 5.** 90% probability contours for parameters indicating spectral hardness. Main pulse: solid contour, secondary pulse: dashed, 'off-pulse': dotted. The abscissas are plotted so that in both columns hard spectra are indicated by confidence contours on the left hand side and soft spectra by contours on the right hand side.

in each individual data set that the improved $\chi^2_{\rm red}$ is a chance occurence (see Table 2).

### *5.2. Pulse phase resolved spectra*

For pulse phase resolved spectroscopy the data was split into three segments: the main pulse (a) ranging in phase from 0.15 to 0.45 in Fig. 3, marked by its more pronounced asymmetric shape and higher flux at both ends of the spectrum, the secondary pulse (b) ranging from 0.65 to 0.95 and the 'off-pulse' regions (c) covering the rest of the pulse phase. We combined both 'off-pulse' regions, as we could not find significant spectral differences between them.

For all observations the spectral shape below the cutoff energy, represented by the power law, is significantly different for the three segments: the secondary pulse has the hardest spectrum, the 'off-pulse' segment the softest. At higher energies there is no such clear distinction in spectral hardness, only a tendency for the secondary pulse to have a softer spectrum than the main pulse. This behaviour is illustrated in Fig. 5, where the left hand panels show 90% probability contours for the range of photon index $\alpha$ vs. $N_{\rm H}$ for the low energy spectrum. The right hand panels show the spread of values for folding energy $E_F$ vs. cutoff energy $E_C$. The parameters $\alpha$ and $E_F$ are indicators for spectral hardness in the respective energy range.

Analyzing the pulse phase resolved data in the same fashion as the phase averaged spectra, we found that the secondary pulse (b) and the 'off-pulse' interval (c) of the November 1988 observations could be fitted moderately well by continuum spectra without the need for additional line features. In contrast, the main pulse data (a) of Nov 20 and Nov 25, 1988 displayed significant deviations between model and observed data. For the January 1991 observation, line features improve the fit significantly for all phase segments, but still the most significant fea-

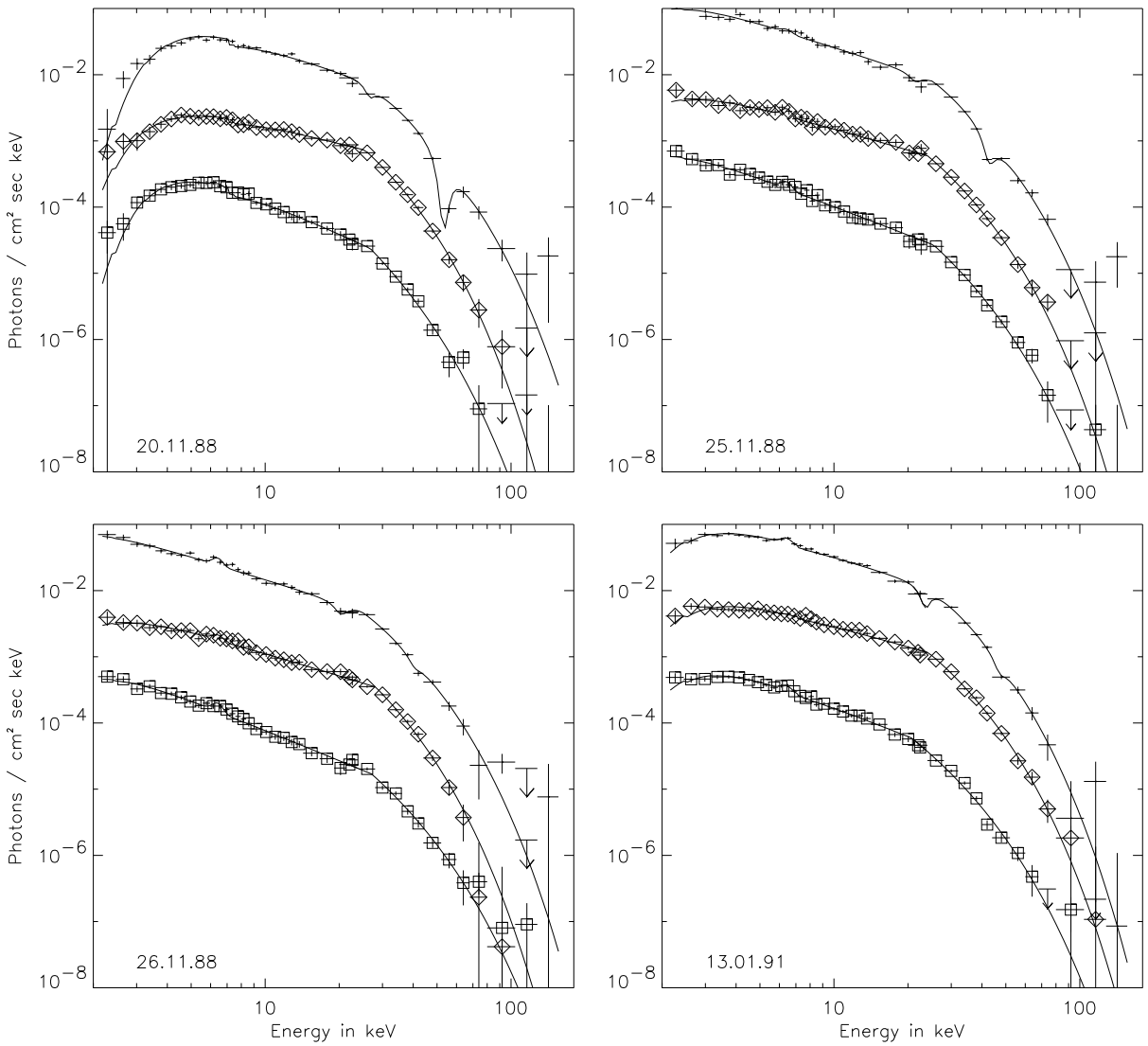


**Fig. 6.** Pulse phase resolved photon spectra for the individual observations. For clarity the spectra of the secondary pulse (◇) and the 'off-pulse' region (□) were multiplied with 0.1 and 0.01 respectively.

tures show up in segment (a). Generally, the features seen in the fits to the phase averaged spectra were mostly due to the contribution of the main pulse data (see Fig. 4).

While cyclotron line features cannot be ruled out for phase segments (b) and (c), there are no significant indications of these in the first three observations and including them into the fitted model led to large uncertainties in the continuum parameters. We therefore present the fit results for these phase segments without line features.

For the three observations of November 1988, the best fit results were obtained using a power law with an exponential cutoff as continuum model, but the above mentioned comptonized models can not be excluded. The last observation was slightly better described by the comptonized models, but note that for this observation a slightly different TTM response matrix was used.

Table 3 gives the best fit parameters of all pulse phase resolved spectra for a power law with an exponential cutoff continuum further modified by two coupled cyclotron lines in the case of phase segment (a). The corresponding photon spectra are shown in Fig. 6.

The best fit values for the line centroid and the relative strengths of the two lines are quite different from observation to observation (see Fig. 6). Still, due to the rather large uncertainties, the different observations are all consistent with a line centroid of $\sim$23 keV and amplitudes of $\sim$0.5 for the fundamental and 0.3–0.8 for the first harmonic. One can take a less conservative estimation of the uncertainties in the line parameters, by assuming no influence of $I_{10\,\mathrm{keV}}$, $N_\mathrm{H}$ and $I_\mathrm{Fe}$ leading to 6 instead of 9 parameters of interest and confidence regions defined by $\chi^2_\mathrm{min}+7.038$ (instead of $\chi^2_\mathrm{min}+10.423$). This yields somewhat smaller parameter ranges but still consistent with the

**Table 3.** Fit results for the phase resolved Vela X-1 spectra. The definition of the phase segments is given in Sect. 5.2). For segments (b) and (c) the parameters of a power law with an exponential cutoff modified by photoelectric absorption and an iron emission line are given. In the case of segment (a) this was further modified by two coupled cyclotron lines (Eq. A1). The reduced $\chi^2$ values obtained with the modified (31 d.o.f.) and the unmodified (34 d.o.f.) continuum are given below the fit results, as well as the probability $Q(F)$ of obtaining the reduction in $\chi^2$ by chance (determined using the $F$-Test). The uncertainties given are 68% ($1\sigma$) confidence limits for joint variations of 9 free parameters ($\chi^2_{\rm min} + 10.423$, see Sect. 3.3).

| | | Nov 20, 1988 | | | Nov 25, 1988 | | | Nov 26, 1988 | | | Jan 13, 1991 | | |
|---|---|---|---|---|---|---|---|---|---|---|---|---|---|
| | | (a) | (b) | (c) | (a) | (b) | (c) | (a) | (b) | (c) | (a) | (b) | (c) |
| normalisation | $I_{10\,\rm keV}$ [1)] | $27^{+2}_{-3}$ | $18^{+1}_{-2}$ | $13^{+1}_{-1}$ | $26^{+2}_{-2}$ | $15^{+2}_{-1}$ | $10^{+1}_{-1}$ | $15^{+1}_{-1}$ | $11^{+1}_{-1}$ | $8^{+0}_{-1}$ | $33^{+2}_{-2}$ | $30^{+1}_{-2}$ | $17^{+1}_{-1}$ |
| photon index | $\alpha$ | $1.3^{+0.3}_{-0.2}$ | $1.0^{+0.1}_{-0.2}$ | $1.7^{+0.2}_{-0.2}$ | $1.2^{+0.2}_{-0.2}$ | $1.1^{+0.1}_{-0.2}$ | $1.4^{+0.2}_{-0.1}$ | $1.2^{+0.2}_{-0.2}$ | $1.1^{+0.1}_{-0.1}$ | $1.5^{+0.1}_{-0.1}$ | $1.2^{+0.2}_{-0.1}$ | $1.0^{+0.2}_{-0.1}$ | $1.4^{+0.1}_{-0.1}$ |
| cutoff energy | $E_C$ [keV] | $26^{+3}_{-8}$ | $25^{+2}_{-1}$ | $27^{+4}_{-4}$ | $25^{+5}_{-3}$ | $24^{+2}_{-2}$ | $25^{+3}_{-2}$ | $25^{+5}_{-3}$ | $28^{+3}_{-3}$ | $27^{+5}_{-4}$ | $25^{+3}_{-3}$ | $24^{+2}_{-2}$ | $21^{+3}_{-3}$ |
| folding energy | $E_F$ [keV] | $16^{+6}_{-5}$ | $10^{+1}_{-1}$ | $12^{+5}_{-3}$ | $13^{+2}_{-2}$ | $11^{+1}_{-1}$ | $13^{+2}_{-2}$ | $14^{+2}_{-2}$ | $11^{+2}_{-2}$ | $15^{+5}_{-5}$ | $12^{+3}_{-2}$ | $12^{+1}_{-1}$ | $13^{+2}_{-2}$ |
| column density | $N_{\rm H}$ [in $10^{22}$] | $18^{+4}_{-4}$ | $11^{+4}_{-4}$ | $16^{+5}_{-4}$ | $2^{+2}_{-2}$ | $2^{+3}_{-2}$ | $1^{+2}_{-1}$ | $2^{+2}_{-2}$ | $2^{+3}_{-2}$ | $2^{+2}_{-2}$ | $5^{+2}_{-2}$ | $5^{+1}_{-2}$ | $5^{+2}_{-2}$ |
| iron line ampl. | $I_{\rm Fe}$ [1)] | $0^{+6}_{-0}$ | $0^{+5}_{-0}$ | $1^{+5}_{-1}$ | $4^{+13}_{-3}$ | $5^{+8}_{-5}$ | $4^{+6}_{-4}$ | $4^{+13}_{-3}$ | $2^{+5}_{-2}$ | $4^{+3}_{-4}$ | $8^{+9}_{-8}$ | $2^{+5}_{-2}$ | $5^{+5}_{-5}$ |
| 1st line center | $E_L$ [keV] | $27^{+2}_{-4}$ | — | — | $21^{+2}_{-2}$ | — | — | $20^{+\infty}_{-\infty}$ | — | — | $24^{+1}_{-3}$ | — | — |
| ampl. 1st line | $A_1$ | $0.5^{+0.5}_{-0.5}$ | — | — | $0.3^{+0.3}_{-0.3}$ | — | — | $0.4^{+0.4}_{-0.4}$ | — | — | $0.8^{+0.4}_{-0.4}$ | — | — |
| ampl. 2nd line | $A_2$ | $2.5^{+6.0}_{-2.5}$ | — | — | $0.9^{+0.8}_{-0.6}$ | — | — | $0.2^{+2.0}_{-0.2}$ | — | — | $0.4^{+1.4}_{-0.4}$ | — | — |
| $\chi^2_{\rm red}$ (31 d.o.f.) | | 1.03 | 0.69 | 1.06 | 1.38 | 0.98 | 0.78 | 1.30 | 0.79 | 1.09 | 1.03 | 1.30 | 0.90 |
| $\chi^2_{\rm red}$ (34 d.o.f.) | | 1.99 | 0.70 | 1.06 | 1.98 | 1.05 | 0.84 | 1.42 | 0.94 | 1.10 | 2.50 | 1.93 | 1.41 |
| $Q(F)$ | | $3.0\cdot10^{-5}$ | 0.32 | 0.40 | $2.6\cdot10^{-3}$ | 0.16 | 0.16 | 0.13 | 0.04 | 0.36 | $1.0\cdot10^{-6}$ | $1.6\cdot10^{-3}$ | $0.7\cdot10^{-3}$ |

[1)] in $10^{-3}$ photons / (cm$^2$ sec keV)

numbers above. The only significant effect is a well defined range ($20^{+3}_{-2}$ keV) for the line centroid in the Nov 26 observation.

While the fit of the model to the data is significantly improved by including cyclotron lines into the model, the uncertainties given for the line parameters show the individual lines to be only marginal. This is due to the fact that including just one of the two possible line features will already result in a fit result within the confidence region defined above. Assuming just a single line feature, the observations of Nov 20 and Nov 25, 1988 would yield a position at 40–60 keV while for Jan 13, 1991 a line at ∼24 keV is more significant. Combining the results of our own analysis, where the evidence slightly favors a feature beyond 40 keV and the results of Makishima et al. (1992) we have chosen to present the fit results for a model with two lines – a fundamental at 20–30 keV and a first harmonic at 40–60 keV.

## 6. Discussion

Since their first detection in the spectrum of Her X-1 (Trümper et al. 1978) cyclotron resonant features have been reported for several accreting pulsars. An overview is given in Parmar (1994).

We find indications for cyclotron scattering features in the broadband spectra of three out of four observations of Vela X-1 with HEXE and TTM, supporting the results of Kendziorra et al. (1992) and the independent Ginga results of Makishima et al. (1992). Looking at the pulse phase resolved spectra we find that these features show up mainly in the spectrum of the phase segment we designated main pulse. A detailed analysis of the Ginga observations (Mihara 1995) found two structures interpreted as cyclotron line features, wich varied in strength over pulse phase. Using a similar designation of pulse phase segments, these features were most significant during the main pulse and relatively weak in other phases. We note that this is in good agreement with our results.

Still, we are concerned that the spectral feature at ∼23 keV coincides with the onset of the spectral cutoff and thus on principle we cannot rule out the possibility of a spurious effect caused by an imperfect description of the continuum. Also, the fit statistics do not allow us to assume the existence of either feature individually with certainty. On the other hand, a feature caused by the continuum should have an effect at all pulse phases but we see pronounced features only in the spectra of the main pulse, supporting the case that these are real lines. Since the statistics of the HEXE/TTM observations do not allow a definite answer, we successfully proposed RXTE observations to resolve these questions.

While the shape of the source continuum varies with pulse phase, it appears to be quite stable from one observation to the next. The main variations are in the overall flux and in the amount of photoelectric absorption. There are indications for variation in the cyclotron line parameters (i.e. the relative strengths of the two harmonics and the position of the line centroid) between the observations, but they are not conclusive. All observations are consistent with constant line strengths and a fundamental at ∼23 keV, corresponding to a magnetic field strength of $2\times10^{12}$ G, an average value for field strengths determined from cyclotron line measurements (Parmar 1994, and references therein).

Due to the low significance of the observed spectral features, an in-depth discussion of the variance in fit parameters over the

pulse phase or from day to day is not feasible. The prominence in one pulse maximum is not surprising since the resonant scattering will lead to more photons scattered out from the line of sight than into this direction when the beamed emission is pointed towards the observer. A more interesting question is, why the scattering features appear to be much more significant in one pulse than in the other, in spite of a relatively similar overall flux in both pulses for the energy range 20–80 keV. This, and the different overall shape of the continuum for the two pulses hints at a different geometry of the emission regions relative to us, since the important interaction cross sections depend on the angle between the magnetic field and the direction of light propagation.

A full modelling of these effects would need to take the gravitational light bending into account (Riffert & Mészáros 1988). Recently, Kraus et al. (1996) have performed such an analysis for Cen X-3 but this is a major effort requiring high quality data over a wide energy range.

The strong pulse-to-pulse variations (Fig. 2) demonstrate that the source is not accreting and emitting in a steady uniform way. Overall flux and spectral hardness can vary significantly between different time intervals corresponding to the same pulse phase. These variations seem to be random with no trends or correlations evident in the analysis, except for the overall pulse phase dependency. In contrast, the overall emission pattern as seen from the profiles averaged over longer time scales seems to be quite stable, mainly varying in overall intensity. Accordingly, even with sensitive instruments care has to be taken to observe this source over adequate integration times if generally applicable results are to be derived.

## Appendix A: analytic form of the best fit spectra

For both sources the best fit results are achieved by a power law with exponential cutoff, modified by photoelectric absorption, an iron emission line and two coupled cyclotron lines, in the form proposed by Tanaka (1986):

$$\begin{aligned} N(E) \;=\; & T(N_{\rm H}, E) \times C(E) \\ & \times \exp\left( -A_1 \frac{(WE/E_L)^2}{(E-E_L)^2 + W^2} \right. \\ & \left. -A_2 \frac{(2WE/2E_L)^2}{(E-2E_L)^2 + (2W)^2} \right) \\ & +\text{gaussian emission line of cold Fe} \end{aligned} \tag{A1}$$

where

$T(N_H, E)$ = transmission of the interstellar medium,

$$C(E) \;=\; \begin{cases} I_0 \cdot \left(\frac{E}{E_0}\right)^{-\alpha} & ; E \le E_C \\ I_0 \cdot \left(\frac{E}{E_0}\right)^{-\alpha} \cdot \exp\left(\frac{E_C - E}{E_F}\right) & ; E > E_C \end{cases} \tag{A2}$$

The parameters are:

| | |
|---|---|
| $E_0$, $I_0$ | normalisation energy and flux |
| $E_C$, $E_F$ | cutoff energy, folding energy |
| $E_{\rm L}$, $W_{\rm L}$ | center energy and HWHM of the absorption line |
| $A_1$, $A_2$ | amplitude of first and second line |

## References


Becker, P. A., Begelman, M. C., 1986, ApJ, 310, 534
Becker, R. H., Rothschild, R. E., Boldt, E. A., et al., 1978, ApJ, 221, 912
Bevington, P. R., Robinson, D. K., 1992, Data Reduction and Error Analysys for the Physical Sciences, McGraw-Hill Book Company
Brinkman, A. C., Dam, J., Mels, W. A., et al., 1985, in Perola & Salvati 1985, 263
Deeter, J. E., Boynton, P. E., Lamb, F. K., Zylstra, G., 1989, ApJ, 336, 376
Döbereiner, S., Maisack, M., Englhauser, J., et al., 1994, A&A, 287, 105
Haberl, F., White, N., 1990, ApJ, 361, 225
Kendziorra, E., Mony, B., Kretschmar, P., et al., 1992, in Tanaka & Koyama 1992, 51
Kraus, U., Blum, S., Schulte, J., et al., 1996, ApJ, 467, 794
Kretschmar, P., Pan, H. C., Kendziorra, E., et al., 1996, A&AS, 120, 175
Lamb, P., Sanford, P., 1979, MNRAS, 188, 555
Lewis, W., Rappaport, S., Levine, A., Nagase, F., 1992, ApJ, 389, 665
Makishima, K., Mihara, T., Nagase, F., Murakami, T., 1992, in Tanaka & Koyama 1992, 23
Mihara, T. 1995, *Ph.D. thesis*, University of Tokyo
Nagase, F. 1989, PASJ, 41, 1
Nagase, F., Hayakawa, S., Masai, K., et al., 1984, ApJ, 280, 259
Nagase, F., Hayakawa, S., Sato, N., 1986, PASJ, 38, 547
Pan, H. C., Kretschmar, P., Skinner, G. K., et al., 1994, ApJS, 92, 448
Parmar, A. 1994, in S. S. Holt, C. S. Day (eds.), The Evolution of X-ray Binaries, No. 308 in AIP Conference Proceedings, 415
Perola, G., Salvati, M., (eds.) 1985, Non-Thermal and Very High Temperature Phenomena in X-Ray Astronomy
Raubenheimer, B. C. 1990, A&A, 234, 172
Reppin, C., Pietsch, W., Trümper, J., et al., 1985, in Perola & Salvati 1985, 279
Riffert, H., Mészáros, P., 1988, ApJ, 325, 207
Skinner, G. K., Pan, H. C., Maisack, M., et al., 1991, A&A, 252, 172
Staubert, R., Kendziorra, E., Pietsch, W., et al., 1980, ApJ, 239, 1010
Sunyaev, R., Titarchuk, L., 1980, A&A, 86, 121
Tanaka, Y. 1986, in D. Mihalas, K. Winkler (eds.), Radiation Hydrodynamics in Stars and Compact Objects, 198–221, Springer-Verlag, Berlin
Tanaka, Y., Koyama, K., (eds.) 1992, Frontiers of X-Ray Astronomy, No. 2 in Frontiers Science Series
Trümper, J., Pietsch, W., Reppin, C., et al., 1978, ApJ, 219, L105


This article was processed by the author using Springer-Verlag LaTeX A&A style file *L-AA* version 3.